Published in final edited form as:
Biomed Microdevices. 2009 August ; 11(4): 773–782. doi:10.1007/s10544-009-9292-x.

Fabrication and physical evaluation of a polymer-encapsulated paramagnetic probe for biomedical oximetry

Guruguhan Meenakshisundaram,
Center for Biomedical EPR Spectroscopy and Imaging, The Ohio State University, Columbus, OH 43210, USA

Departments of Internal Medicine, The Ohio State University, Columbus, OH 43210, USA

Davis Heart and Lung Research Institute, The Ohio State University, Columbus, OH 43210, USA

Edward Eteshola,
Biomedical Engineering, The Ohio State University, 473 West 12th Avenue, DHLRI, Room: 305C, Columbus, OH 43210, USA

Davis Heart and Lung Research Institute, The Ohio State University, Columbus, OH 43210, USA

Ramasamy P. Pandian,
Center for Biomedical EPR Spectroscopy and Imaging, The Ohio State University, Columbus, OH 43210, USA

Departments of Internal Medicine, The Ohio State University, Columbus, OH 43210, USA

Davis Heart and Lung Research Institute, The Ohio State University, Columbus, OH 43210, USA

Anna Bratasz,
Center for Biomedical EPR Spectroscopy and Imaging, The Ohio State University, Columbus, OH 43210, USA

Departments of Internal Medicine, The Ohio State University, Columbus, OH 43210, USA

Davis Heart and Lung Research Institute, The Ohio State University, Columbus, OH 43210, USA

Stephen C. Lee, and
Biomedical Engineering, The Ohio State University, 473 West 12th Avenue, DHLRI, Room: 305C, Columbus, OH 43210, USA e-mail: lee.1996@osu.edu

Davis Heart and Lung Research Institute, The Ohio State University, Columbus, OH 43210, USA

Periannan Kuppusamy
Center for Biomedical EPR Spectroscopy and Imaging, The Ohio State University, Columbus, OH 43210, USA

Departments of Internal Medicine, The Ohio State University, Columbus, OH 43210, USA

Davis Heart and Lung Research Institute, The Ohio State University, Columbus, OH 43210, USA

Abstract

Lithium octa-*n*-butoxynaphthalocyanine (LiNc-BuO) is a promising probe for biological electron paramagnetic resonance (EPR) oximetry and is being developed for clinical use. However, clinical applicability of LiNc-BuO may be hindered by potential limitations associated with biocompatibility,

Correspondence to: Stephen C. Lee.

biodegradation, and migration of individual crystals in tissue. To overcome these limitations, we have encapsulated LiNc-BuO crystals in polydimethyl siloxane (PDMS), an oxygen-permeable and bioinert polymer, to fabricate conveniently implantable and retrievable oxygen-sensing chips. Encapsulation was performed by a simple cast-molding process, giving appreciable control over size, shape, thickness and spin density of chips. The *in vitro* oxygen response of the chip was linear, reproducible, and not significantly different from that of unencapsulated crystals. Cast-molding of the structurally-flexible PDMS enabled the fabrication of chips with tailored spin densities, and ensured non-exposure of embedded LiNc-BuO, mitigating potential biocompatibility/toxicological concerns. Our results establish PDMS-encapsulated LiNc-BuO as a promising candidate for further biological evaluation and potential clinical application.

Keywords

EPR oximetry; Oxygen sensor; Particulate probe; Encapsulation; Polymer coating; Biocompatible EPR probe

1 Introduction

Oxygen is essential to all aerobic life, and tissue pO_2 is a key parameter in many pathophysiological conditions, including ischemic diseases, reperfusion injury, oxygen toxicity, cancer, peripheral vascular disease, and wound healing (Hopf and Rollins 2007; Kulkarni et al. 2007; Kutala et al. 2007; Marso and Hiatt 2006; Vaupel et al. 2007). *In vivo* measurement of molecular oxygen is crucial for effective diagnosis and treatment of multiple disease states. Among methods available for measuring oxygen concentration (Springett and Swartz 2007; Vikram et al. 2007), electron paramagnetic resonance (EPR) oximetry offers unique advantages, including reliable, repeatable, real-time reporting of oxygenation/redox status in biological tissues without consumption of O_2. EPR oximetry is the only minimally-invasive technique that provides absolute values of oxygen concentration in tissue (Khan et al. 2007; Swartz 2004). The ability of EPR to make iterative measurements of the oxygen partial pressure (pO_2), from a single tissue site, depends on the availability of water-insoluble crystalline EPR probes (Dunn and Swartz 2003), such as lithium phthalocyanine (LiPc) (Liu et al. 1993), lithium naphthalocyanine (LiNc) (Ilangovan et al. 2002), and lithium octa-*n*-butoxynaphthalocyanine (LiNc-BuO) (Pandian et al. 2003b).

These particulate EPR probes can all be used in their neat crystalline form to sense molecular oxygen (Ilangovan et al. 2002; Liu et al. 1993; Pandian et al. 2003b), but may have limitations associated with particle migration within the tissue, (diffusing and decreasing EPR signal over time) and, potentially, with biocompatibility and toxicity of particles directly exposed to tissue. Also, exposure of some probes (particularly LiPc and LiNc) to the *in vivo* environment degrades their oximetry properties over time (Ilangovan et al. 2002; Liu et al. 1993). Successful transformation of EPR oximetry into a powerful clinical tool requires stabilization of probes, in space, in tissue sites, protection of probes from degradative conditions *in vivo*, and sequestering probes and tissue to mitigate potential toxicity. We, and others, approach this set of challenges by encapsulating crystalline EPR probes in biocompatible, biostable, gas-permeable polymer matrices (Dinguizli et al. 2006; Dinguizli et al. 2008; Eteshola et al. 2009; Gallez et al. 1999; Gallez and Mader 2000; He et al. 2001).

In the past, coating of particulate carbon materials using a number of biopolymers (Gallez et al. 1999; He et al. 2001), and LiPc using Teflon AF 2400 (TAF), cellulose acetate (CA) and polyvinyl acetate (PVAc), have been reported (Dinguizli et al. 2006; Eteshola et al. 2009). Some critical polymer parameters that need to be considered in the development of encapsulated oximetry probes include cost of the encapsulating polymer, film casting/

fabrication properties, handling/mechanical properties of polymer films, and film oxygen permeability (Eteshola et al. 2009). From the standpoint of all of these considerations, PDMS is a desirable polymer for encapsulation of oximetry probes. It is a biocompatible, highly flexible, and highly oxygen permeable silicone polymer (Mata et al. 2005) that has been used in a wide range of medical device and health care applications (Abbasi et al. 2001), and so is extremely well-studied. PDMS has been approved for use in human subjects and is one of the reference materials provided by the National Heart Lung and Blood Institute for standardized biocompatibility testing (Belanger and Marois 2001). LiNc-BuO is the EPR probe used in this study, since it offers some unique advantages over other crystalline probes for oximetry applications, including long-term stability and responsiveness to oxygen *in vivo*, high spin density, and excellent *in vitro* applicability (Kutala et al. 2004; Pandian et al. 2003a, b; Wisel et al. 2007).

Coating of particulate EPR probes (LiPc) using TAF was performed by solvent evaporation approaches, which produced very thin TAF films (Eteshola et al. 2009). While the oximetry properties of TAF-encapsulated LiPc were very good, the handling properties of the films were inconvenient. Thin TAF films were so brittle that maintaining them intact during implantation and explantation was a challenge. Breakage of TAF films, *in vivo*, could prevent removal of the entire oximetry chip after completion of oxygen-monitoring, and thereby potentially exacerbate any inflammatory, immunological or toxicological hazard presented by the exposed oximetry probe. To overcome these operational difficulties, we have used a simple and easy-to-use cast-molding and polymerization method, using PDMS, which allowed for the fabrication of mechanically-robust EPR probe encapsulations. The method also provided the capability of covering the embedded oximetry crystals with multiple layers of PDMS for fully sequestering them from the *in vivo* environment, and improving their biotolerability. Thick, multilayer TAF encapsulation of oximetry particles was not feasible, owing to the low solubility of TAF in the available solvents (Eteshola et al. 2009).

To enhance the suitability of LiNc-BuO for clinical EPR oximetry, we have developed conveniently implantable and retrievable formulations (chips) of microcrystalline LiNc-BuO by encapsulating the probe in PDMS, using a cast-molding and polymerization approach. For the sake of simplicity, we will use the acronym ‘LiNc-BuO:PDMS’ to refer to the chips made by the encapsulation of LiNc-BuO in PDMS. We describe fabrication and *in vitro* oximetry evaluation of LiNc-BuO:PDMS. We also evaluate the physical (material and surface) properties of this new probe-polymer composite.

2 Materials and methods

2.1 Synthesis of LiNc-BuO and fabrication of LiNc-BuO: PDMS chips

LiNc-BuO was synthesized as microcrystalline powder as reported (Pandian et al. 2003b). Polydimethyl siloxane (PDMS) was obtained as medical grade Silastic (MDX4-4210) from Dow Corning (Midland, MI). LiNc-BuO: PDMS (Fig. 1) was fabricated by cast-molding and polymerization. Silastic was mixed at recommended base-catalyst ratio (10:1), and crystals of LiNc-BuO were thoroughly dispersed into this mixture using a spatula. The base-catalyst/ LiNc-BuO microcrystal mixture was degassed under vacuum and poured into hexagonal polystyrene weighing boats. The degassed mixture was cured in an oven at 75°C for 7 h. Smaller pieces, of various sizes (from 0.5 to 2 mm) were cut from larger LiNc-BuO:PDMS chips. A pure PDMS film, without LiNc-BuO crystals (Fig. 1), was fabricated for comparison to the LiNc-BuO: PDMS chip. Fabrication of the pure PDMS film was carried out as described for LiNc-BuO:PDMS chips, except that LiNc-BuO crystals were omitted.

2.2 Evaluation of the density and distribution of LiNc-BuO spins in LiNc-BuO:PDMS

LiNc-BuO:PDMS samples were fabricated with four different spin densities, by loading 5, 10, 20, and 40 mg of LiNc-BuO microcrystals (mean crystal-size: ~50μm (Pandian et al. 2006; Pandian et al. 2003b)), each into 5.5 g of PDMS (base-catalyst mixture). These four formulations of LiNc-BuO:PDMS are called C-5, C-10, C-20, and C-40. Numbers after the hyphen indicate the mass of LiNc-BuO particulates (in mg) loaded.

Spin density was determined using X-band EPR spectroscopy, by comparing the area under the curve (AUC) of the first-derivative EPR spectra of the four chip formulations with the AUC of a standard of known spin density (triarylmethyl radical, TAM) (Kutala et al. 2004). The four samples (C-5, C-10, C-20, and C-40) were weighed for normalization of spin densities to LiNc-BuO:PDMS mass. EPR spectra of LiNc-BuO:PDMS chips and TAM were obtained at the same instrument settings to enable direct comparison and spin density calculation.

Spin distribution was evaluated via X-band EPR imaging. Two-dimensional images of surfaces of the four samples were obtained using a Bruker Elexsys E580 spectrometer (Billerica, MA). Samples, for imaging, were made anoxic by sealing them in glass EPR tubes containing sodium hydrosulfite (sodium hydrosulfite absorbs molecular oxygen). Samples were made anoxic to avoid oxygen-induced line-broadening in order to enhance signal-to-noise ratio, and minimize image acquisition time. Image acquisition was performed using the following parameters: resolution, 10μm; field-of-view, 4 mm; magnetic field gradient, 44.3 G/cm; modulation amplitude, 0.32 G; sweep width, 20 G; sweep time, 10 s.

Oxygen calibration was performed for the four different formulations of LiNc-BuO:PDMS to evaluate the effect, if any, of increasing spin density on the oxygen response.

2.3 Surface evaluation of LiNc-BuO:PDMS using atomic force microscopy (AFM)

LiNc-BuO:PDMS chips (40 mg LiNc-BuO in 5.5 g PDMS) and clear films of PDMS, without LiNc-BuO, were used for surface analysis. Surface characterization was performed using a multimode atomic force microscope with a Nanoscope III controller (Digital Instruments, Santa Barbara, CA). Samples were rinsed clean with distilled water to remove any dirt on the surface, and dried completely under vacuum, before contact-mode AFM measurements were made. Surface roughness was estimated using the roughness analysis tool in the software (Digital Instruments, Santa Barbara, CA).

2.4 Oxygen calibration

Peak-to-peak linewidths of the first-derivative EPR spectra of uncoated LiNc-BuO and LiNc-BuO:PDMS samples were measured at different partial pressures of oxygen (pO_2). EPR measurements were performed using a Bruker ER-300 spectrometer, operating at X-band (9.8 GHz). Spectrometer settings were: microwave power, 1 mW; modulation frequency, 100 kHz, receiver time constant, 0.04 s, acquisition time, 36 s (3×12-s scans). Modulation amplitude was adjusted to one-third or less of the linewidth. Acquisition and analysis of spectra were carried out using custom-developed software packages, (EPR 2000 and AutoLinewidth, developed in-house) Oxygen calibration of unencapsulated LiNc-BuO was also obtained to enable comparison with LiNc-BuO:PDMS. Pressurized cylinders containing known proportions of pre-mixed nitrogen and oxygen were used to expose the samples to different oxygen environments, ranging from 0 to 160 mmHg. Samples were secured in place in glass EPR tubes, with both ends open, and equilibrated with gas at a flow rate of 2 l/min. The glass EPR tube was placed in the resonator cavity so that the sample was at the center of the active resonator volume. The calibration curve was constructed by plotting the linewidth values obtained against the oxygen concentrations used. The slope of the calibration curve (which equals the oxygen sensitivity), was estimated by fitting a straight line to the data points.

2.5 Evaluation of oxygen time-response

The temporal responsiveness of LiNc-BuO:PDMS to changes in pO_2 was tested in two ways: by switching the bulk gas (flowing past the sample) from room air to nitrogen and also by inducing rapid fluctuations in oxygen partial pressure using an oscillator-driven speaker-diaphragm setup as reported (Vikram et al. 2008).

To rapidly switch between flowing gases, a manual three-way valve was used. The two input lines to the valve were connected to gas cylinders containing pure nitrogen and room air. The output of the valve was connected to the EPR tube containing the sample. All the connections were sealed using Parafilm to avoid any leaks. The magnetic field, for acquisition, was set at the peak of the spectrum under nitrogen equilibration. The input gas was switched manually between room air and nitrogen at periodic intervals, as decided by the nature and response of the sample.

Samples were also subjected to sinusoidal changes in pO_2 at frequencies up to 300 Hz, using a previously described speaker-diaphragm apparatus (Vikram et al. 2008). In brief, a function generator was used to drive a speaker, the center cone of which was attached to a piston.

The piston was then brought into contact with a diaphragm, made of a laboratory-grade nitrile exam glove (Fisher Scientific, Pittsburgh, PA) stretched over a plastic tube, which was in turn connected to a glass EPR tube. The sample was placed in the glass EPR tube, and the system was closed. The spatial displacement of the diaphragm due to the movement of the piston by the speaker cone induced a change in volume in the closed system, and, therefore, changed system pO_2. EPR acquisition and data analysis were performed as described (Vikram et al. 2008).

2.6 Statistical analysis

Data were expressed as mean ± SD and compared using a Student's t-test with the level of significance (p) set at 0.05.

3 Results and discussion

3.1 Fabrication of LiNc-BuO:PDMS chips

Fabrication of LiNc-BuO:PDMS is straightforward, and could be done in most laboratories without special equipment. LiNc-BuO:PDMS chips were fabricated in a variety of sizes and shapes by cast-molding and polymerization (Fig. 1). Panel (a) shows a PDMS film lacking LiNc-BuO microcrystals for comparison with LiNc-BuO: PDMS chip shown in Panel (b). Panels (c) and (d) demonstrate our ability to fabricate these chips in different sizes, shapes; with different thicknesses and varying amounts of LiNc-BuO (color intensity is directly related to ratio of the masses of LiNc-BuO microcrystals and PDMS).

As LiNc-BuO is a particulate material, the distribution of the compound in the polymer matrix cannot be entirely homogenous. The uniformity of LiNc-BuO distribution within the PDMS matrix is dependent on the relative masses of the crystals and the base-catalyst mixture (polymer), and the thoroughness of hand-mixing of polymer with oximetry particles. Imperfect uniformity of LiNc-BuO distribution is apparent in the circular chip in the center of Panel (c) (Fig. 1).

Cast-molding and polymerization methods are more convenient for embedding particles in polymer than are our recently-described solvent evaporation approach for encapsulation of crystalline EPR oximetry probes (Eteshola et al. 2009). Solvent evaporation approaches are limited by the solubilities of both the polymer and the oximetry crystals in solvent. Oximetry

properties of phthalocyanine compounds, such as LiNc-BuO, depend on their intact crystal structure. Solubility of oximetry crystals leads to their dissolution and loss of oxygen sensitivity. On the other hand, limited solubility of polymer restricts the mass of polymer that can be deposited, thereby minimizing the thickness of the polymer films that can be made (Eteshola et al. 2009). Cast-molding using PDMS enabled us to overcome these limitations and fabricate chips of defined size, shape, and thickness.

3.2 Density and distribution of LiNc-BuO spins in the chip

Spin density was determined by comparing AUC values of first-derivative EPR spectra of the four LiNc-BuO:PDMS formulations *viz*. C-5, C-10, C-20 and C-40 (Fig. 2, Panel (a)), with the AUC of the first-derivative EPR spectrum of a known standard (TAM). There is a linear correlation between the mass of LiNc-BuO loaded into the PDMS matrix and chip spin density, as expected. As discussed above, the particulate nature of LiNc-BuO precludes perfectly homogeneous distribution of the probe in PDMS. However, EPR imaging offers a direct means to visualize the uniformity of spin distribution in the LiNc-BuO:PDMS chip.

Panel (b) shows representative 2-dimensional EPR images of the four chip formulations. In general, EPR image intensities (brightness of color) are congruent with the linear trend in measured spin densities seen in Fig. 2, Panel (a). These high resolution (10μm) EPR images suggest that LiNc-BuO spins are fairly evenly distributed within the PDMS matrix. The unusually bright regions (especially in the image corresponding to C-10) may be due to clumping of LiNc-BuO crystals at that location during the curing process. This could be mitigated by thorough dispersion of the LiNc-BuO crystals in the PDMS base-catalyst mixture before it cures.

3.3 Surface analysis

We used AFM to compare the surfaces of the LiNc BuO: PDMS chip and a pure PDMS chip (without LiNc-BuO). We reasoned that if LiNc-BuO crystals were exposed on the surface of the LiNc-BuO:PDMS chip, it would be differentiable from the surface of a pure PDMS chip. Specifically, in that case, we expected that the chip surface would be rougher than the surface of the pure PDMS chip. We evaluated the surface features of intact and sectioned (cut) surfaces of either chip (LiNc-BuO:PDMS and pure PDMS). Representative AFM images of the intact surface of a pure PDMS chip (control) and a LiNc-BuO:PDMS chip (40 mg of LiNc-BuO in 5.5 g PDMS), are shown in the top row of Fig. 3, Panel (a). RMS roughness of the two surfaces was not significantly different (Panel (b)).

Representative AFM images of the sectioned (cut) surface of either chip are shown in the bottom row of Panel (a). The cut surface of the LiNc-BuO:PDMS chip is substantially more irregular than the cut surface of a pure PDMS chip. This relative increase in RMS roughness is statistically significant ($p<0.05$) and corroborates rough-ness assessed qualitatively in the AFM images. We suspect the difference in roughness to be due to a combination of LiNc-BuO crystals protruding from the cut chip surface and voids left in the chip surface left by “pluck out” of crystals occurring when the chip was cut.

The comparable surface regularity of uncut pure PDMS and uncut LiNc-BuO:PDMS chip surfaces, particularly in contrast with the relative roughnesses of the cut surfaces of the two, suggests that LiNc-BuO crystals were not exposed on the surfaces of LiNc-BuO:PDMS uncut chips, and so are not expected to be directly exposed to tissue when implanted *in vivo*. In addition, the oxygen-sensing properties of intact chips were not significantly different from that of cut chips (data not shown), suggesting that the oxygen-sensing by the chip does not depend on crystals exposed on the surface by cutting.

Any potential exposure of embedded LiNc-BuO crystals can be eliminated by sequential deposition of multiple layers of PDMS on an existing/cut LiNc-BuO:PDMS chip surface. This is achieved more conveniently using the cast-molding and polymerization method, than using the previously-reported solvent evaporation approach. Solvent evaporation methods, especially using TAF, led to very thin oximetry films (Eteshola et al. 2009). The application of multiple polymer coatings by solvent evaporation is also hindered by the risk of solubilizing previously deposited polymer layers, limiting achievable film thickness.

3.4 Oxygen calibration

EPR linewidth response of LiNc-BuO:PDMS chips to molecular oxygen were determined for all four chip formulations. In all cases, oxygen responses of LiNc-BuO:PDMS chips were linear over the tested pO_2 range (0 to 160 mmHg). Linewidth response of the C-10 chip, which was typical of all four LiNc-BuO:PDMS chip formulations, and the response of unencapsulated LiNc-BuO crystals (for comparison) is shown in Fig. 4. The C10 chip response was comparable to that of unencapsulated crystals across the tested pO_2 range. Oxygen sensitivities (i.e., the slope of the pO_2 calibration curve) of C-10 LiNc-BuO:PDMS (7.65±0.07 mG/mmHg) and unencapsulated LiNc-BuO crystals (7.54±0.10 mG/mmHg) were not significantly different. The oxygen-sensing characteristics (linearity and slope of calibration) of the four LiNc-BuO:PDMS formulations (C-5, C-10, C-20 and C-40) were identical and highly comparable to those of neat LiNc-BuO crystals (Data not shown). Therefore, PDMS encapsulation did not significantly alter oxygen calibration of LiNc-BuO crystals.

PDMS was not saturated up to a pO_2 of 160 mmHg, as suggested by the fact that the oxygen sensitivities of encapsulated and unencapsulated LiNc-BuO crystals are not significantly different (Fig. 4). At pO_2 levels high enough to saturate the PDMS matrix, encapsulated LiNc-BuO would experience a lower oxygen concentration (that which saturates PDMS) than would unencapsulated crystals in the same testing environment (unencapsulated crystals experiencing the environmental oxygen concentration), and significant differences in oxygen sensitivity between encapsulated and unencapsulated crystals might be observed. However, for most *in vivo* applications of the LiNc-BuO: PDMS chip, normal physiological tissue pO_2 is unlikely to be higher than 160 mmHg. As a result, the trustworthiness of oxygen-sensing by LiNc-BuO over all practical *in vivo* pO_2 levels is not significantly compromised by PDMS encapsulation.

3.5 Oxygen time-response

Oxygen calibration of unencapsulated and PDMS-encapsulated LiNc-BuO is broadly comparable, but one would expect that the kinetics of the pO_2 response to differ between encapsulated and unencapsulated LiNc-BuO crystals. Oxygen must transit the PDMS layer prior to encountering LiNc-BuO crystals. Diffusion through PDMS (or any other polymer matrix) requires time, and so oxygen responses of LiNc-BuO:PDMS should accrue more slowly than oxygen responses by uncoated crystals. We demonstrated this by comparing the response time of LiNc-BuO:PDMS chip to changes in pO_2 to that of neat LiNc-BuO crystals via EPR spectroscopy.

Panel (a) of Fig. 5 shows the time-response of uncoated LiNc-BuO crystals to switching of the flowing gas, from nitrogen (0% O_2) to room air (20.9% O_2) and *vice versa*. The response-time for switching from nitrogen to room air was less than 1 s, while that for the switching from room air to nitrogen was about 3 s. The response was reproducible, as can be seen from the number of cycles shown in Panel (a), indicating that the gas-switching did not affect the oxygen-sensing ability of the probe.

We expected the response of the chip to gas flow-switching to be measurably slower than the response of uncoated LiNc-BuO. In a switch from room air to nitrogen, the response of LiNc-

BuO:PDMS was slower than that of uncoated PDMS (Fig. 5, Panel (b)). The difference between alacrity of EPR-detectable oximetry responses between uncoated LiNc-BuO and LiNc-BuO:PDMS was most pronounced for the transition from room air to nitrogen. LiNc-BuO:PDMS chips responded over about 120 s, as opposed to a response-time of approximately 3 s for uncoated LiNc-BuO. The change from nitrogen to room air was sensed much faster by the chip, with a response time of approximately 5 s. Several cycles of gas-switching response were recorded (data not shown), and confirmed that the temporal response of the LiNc-BuO:PDMS chip was reproducible. Only one cycle is shown in the figure for convenient visual comparison with the uncoated probe response in Panel (a).

The disparity in response times between unencapsulated LiNc-BuO and chip was apparent from the manual gas-flow switching experiment (Fig. 5). However, these experiments were limited by the minimal time required for an operator to open and close gas supply valves. This potentially resulted in slight overestimation of the response times: the EPR response may change faster than it was possible to manually manipulate gas supply valves (between 1 and 2 s). The response time of the chip when the gas was switched from oxygen to nitrogen was long enough (120 s) that the time to manually switch gas (1–2 s) did not significantly affect it, but may affect the response time when switching from nitrogen to oxygen (5 s). The speed of responses to changes in pO_2 can be measured with greater accuracy using audio speaker-mediated pressure modulation, as previously described (Vikram et al. 2008). This system produces very rapid and controllable fluctuations in pO_2 (on the order of 200 Hz, for changes in pO_2 of 20 mmHg or less (Vikram et al. 2008)).

LiNc-BuO:PDMS responded in 5±0.3 ms (200 Hz) to pO_2 fluctuations. This value was comparable to, though measurably slower than, the reported response time of uncoated LiNc-BuO (< 3.3 ms) (Vikram et al. 2008). The minimal reported time scale of oxygen changes *in vivo* is less than 0.1 Hz, as reported for tumors in mice (Baudelet et al. 2004; Brurberg et al. 2004; Brurberg et al. 2003). LiNc-BuO:PDMS chips responded more rapidly (200 Hz) than pO_2 is reported to increase *in vivo* (100 Hz or slower), and therefore LiNc-BuO:PDMS chips, can be used to accurately follow kinetics of increasing oxygen perfusion that is likely to be encountered *in vivo*. Since the responses of LiNc-BuO:PDMS chips to decreasing oxygen follow much slower kinetics than neat LiNc-BuO crystals, neat LiNc-BuO crystals may be preferable to LiNc-BuO:PDMS chips in applications whose objective is tracking rapid decreases in pO_2.

4 Conclusions

We have demonstrated the fabrication and initial testing of biocompatible EPR oximetry sensors, LiNc-BuO:PDMS chips, made by the encapsulation LiNc-BuO probes in PDMS by a cast-molding and polymerization method. The cast-molding method is superior to our previously reported solvent evaporation method in that it allowed convenient fabrication of chips in any chosen shape or thickness, and allowed deposition of multiple layers of polymer. Encapsulation of LiNc-BuO with PDMS precludes LiNc-BuO crystals from direct contact with tissue. The oxygen calibration of the embedded particulates was not affected by encapsulation, which also allowed fabrication of chips with controllable spin densities. While oxygen-time response of LiNc-BuO was increased by encapsulation, response times were acceptable for *in vivo* applications to track increases in oxygenation. AFM imaging was used to demonstrate that LiNc-BuO crystals were embedded in the polymer matrix of the chip. Crystals were not exposed on the chip surfaces except cut surfaces. Furthermore, surface-exposed LiNc-BuO crystals were not necessary for oximetry: oxygen sensitivity of cut and uncut chips were identical. Thus we have developed a novel EPR oximetry probe, the LiNc-BuO:PDMS chip, with potential for further pre-clinical evaluation and eventual clinical application.

Acknowledgments

This study was supported by National Institutes of Health (NIH) grant EB004031. We would like to thank Daniel Iscru and Gunjan Agarwal at the AFM core lab, Ohio State University Medical Center for AFM data acquisition and roughness analysis.

References

Abbasi F, Mirzadeh H, Katbab AA. Polym. Int 2001;50(12):1279–1287.

Baudelet C, Ansiaux R, Jordan BF, Havaux X, Macq B, Gallez B. Phys. Med. Biol 2004;49:3389–3411. [PubMed: 15379021]

Belanger MC, Marois Y, Biomed J. Mater. Res 2001;58(5):467–477.

Brurberg KG, Graff BA, Olsen DR, Rofstad EK. Int. J. Radiat. Oncol. Biol. Phys 2004;58(2):403–409. [PubMed: 14751509]

Brurberg KG, Graff BA, Rofstad EK. Br. J. Cancer 2003;89(2):350–356. [PubMed: 12865929]

Dinguizli A, Jeumont S, Beghein N, He J, Walczak T, Lesniewski PN, Hou H, Grinberg OY, Sucheta A, Swartz HM, Gallez B. Biosens. Bioelectron 2006;21(7):1015–1022. [PubMed: 16368480]

Dinguizli M, Beghein N, Gallez B. Physiol. Meas 2008;29(11):1247–1254. [PubMed: 18843166]

Dunn JF, Swartz HM. Methods 2003;30(2):159–166. [PubMed: 12725782]

Eteshola E, Pandian RP, Lee SC, Kuppusamy P. Biomed. Micro-devices. 2009(Epub ahead of print)

Gallez B, Jordan BF, Baudelet C. Magn. Res. Med 1999;42(1):193–196.

Gallez B, Mader K. Free Radic. Biol. Med 2000;29(11):1078–1084. [PubMed: 11121714]

He J, Beghein N, Ceroke P, Clarkson RB, Swartz HM, Gallez B. Magn. Res. Med 2001;46(3):610–614.

Hopf HW, Rollins MD. Antioxid. Redox. Signal 2007;9(8):1183–1192. [PubMed: 17536961]

Ilangovan G, Manivannan A, Li HQ, Yanagi H, Zweier JL, Kuppusamy P. Free Radic. Biol. Med 2002;32 (2):139–147. [PubMed: 11796202]

Khan N, Williams BB, Hou H, Li H, Swartz HM. Antioxid. Redox. Signal 2007;9(8):1169–1182. [PubMed: 17536960]

Kulkarni AC, Kuppusamy P, Parinandi N. Antioxid. Redox. Signal 2007;9(10):1717–1730. [PubMed: 17822371]

Kutala VK, Parinandi NL, Pandian RP, Kuppusamy P. Antioxid. Redox. Signal 2004;6(3):597–603. [PubMed: 15130286]

Kutala VK, Khan M, Angelos MG, Kuppusamy P. Antioxid. Redox. Signal 2007;9(8):1193–1206. [PubMed: 17571958]

Liu KJ, Gast P, Moussavi M, Norby SW, Vahidi N, Walczak T, Wu M, Swartz HM. Proc. Natl. Acad. Sci. USA 1993;90(12):5438–5442. [PubMed: 8390665]

19. Marso SP, Hiatt WR. J. Am. Coll. Cardiol 2006;47(5):921–929. [PubMed: 16516072]

Mata A, Fleischman AJ, Roy S. Biomed. Microdevices 2005;7(4):281–293. [PubMed: 16404506]

Pandian RP, Kutala VK, Parinandi NL, Zweier JL, Kuppusamy P. Arch. Biochem. Biophys 2003a;420 (1):169–175. [PubMed: 14622987]

Pandian RP, Parinandi NL, Ilangovan G, Zweier JL, Kuppusamy P. Free Radic. Biol. Med 2003b;35(9): 1138–1148. [PubMed: 14572616]

Pandian RP, Kim YI, Woodward PM, Zweier JL, Manoharan PT, Kuppusamy P, Mater J. Chem 2006;16 (36):3609–3618.

Springett R, Swartz HM. Antioxid. Redox. Signal 2007;9(8):1295–1301. [PubMed: 17576162]

Swartz HM. Antioxid. Redox. Signal 2004;6(3):677–686. [PubMed: 15130295]

Vaupel P, Hockel M, Mayer A. Antioxid. Redox. Signal 2007;9(8):1221–1235. [PubMed: 17536958]

Vikram DS, Zweier JL, Kuppusamy P. Antioxid. Redox. Signal 2007;9(10):1745–1756. [PubMed: 17663644]

Vikram DS, Ahmad R, Pandian RP, Petryakov S, Kuppusamy P. J. Magn. Res 2008;193(1):127–132.

Wisel S, Chacko SM, Kuppusamy ML, Pandian RP, Khan M, Kutala VK, Burry RW, Sun B, Kwiatkowski P, Kuppusamy P. am. J. Physiol. Heart. Circ. Physiol 2007;292(3):H1254–H1261. [PubMed: 17142337]

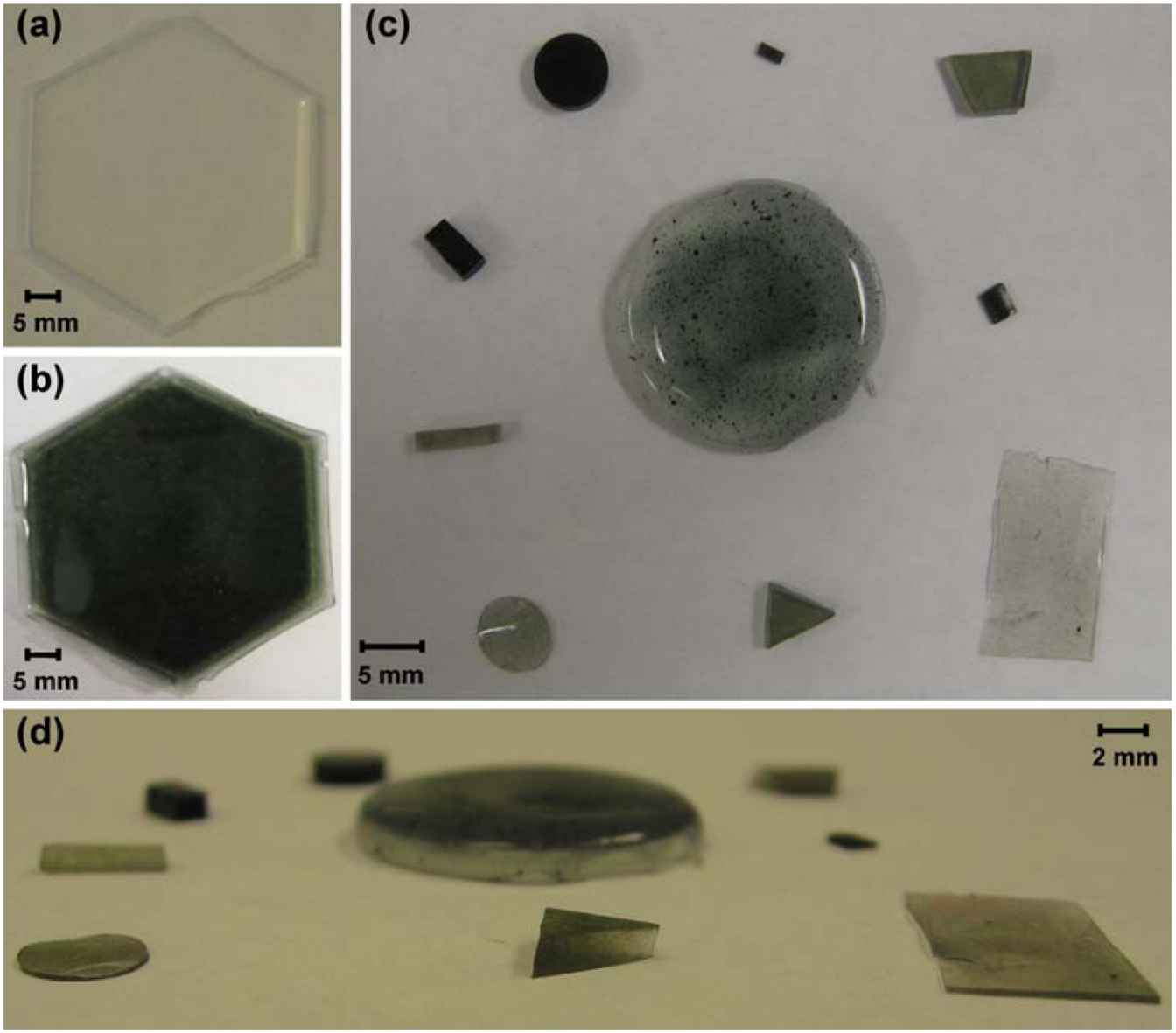

Fig. 1.

Chips fabricated by the encapsulation of LiNc-BuO particulates in PDMS. LiNc-BuO:PDMS chips were made by cast-molding and polymerization, by dispersing the LiNc-BuO crystals in the uncured polymer base-catalyst mixture and curing at 75°C for 7 h. Control (pure) PDMS films, lacking LiNc-BuO crystals, were made using the same procedure, but without adding any particulates. **(a)** Pure PDMS film without particulates **(b)** LiNc-BuO:PDMS chip fabricated with 40 mg of LiNc-BuO in 5.5 g of PDMS. **(c)** Pieces of LiNc-BuO:PDMS with varying sizes, shapes and ratios of particulate to polymer (top view) **(d)** Side view of **(c)**. Photographs demonstrate the successful fabrication of LiNc-BuO:PDMS chips in different shapes and sizes, with different thicknesses and varying amounts of LiNc-BuO

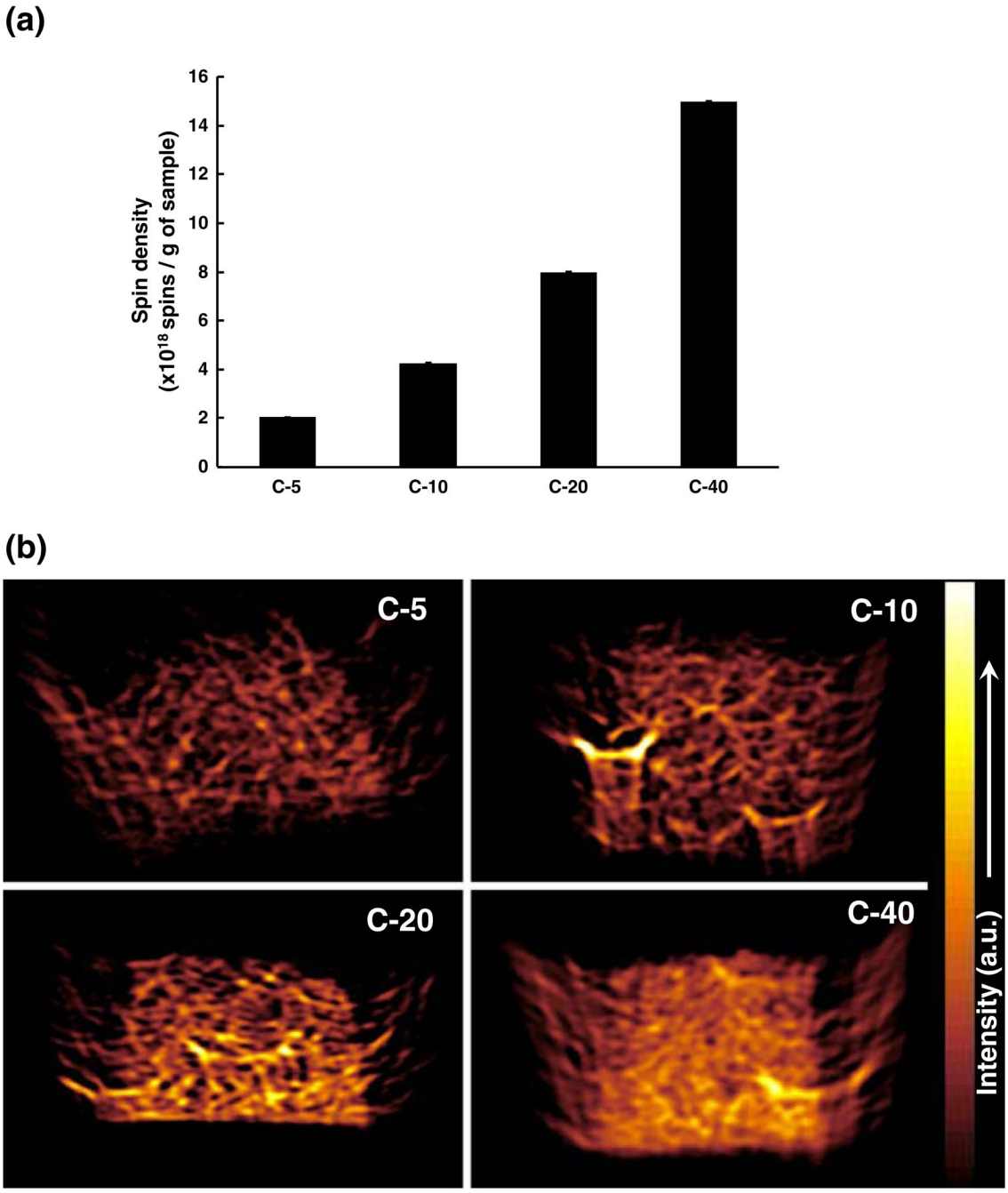

Fig. 2.

LiNc-BuO:PDMS chips with increasing spin density. Four different formulations of LiNc-BuO:PDMS, viz. C-5, C-10, C-20, and C-40, were fabricated by incorporating 5, 10, 20 and 40 mg of LiNc-BuO, respectively, in the same amount of PDMS (5.5 g). **(a)** Spin density of the LiNc-BuO:PDMS chip formulations. Spin density was evaluated, using a pre-calibrated standard, at X-band (9.8 GHz). Results (mean ± SD, *n*=3), normalized by sample weight, show a linear relationship between mass of particulates incorporated and spin density of the four chip formulations. The calculated spin densities per g of chip weight, of the formulations were also consistent with the spin density of unencapsulated LiNc-BuO, per mg of LiNc-BuO, reported previously (Pandian et al. 2003b). **(b)** X-band EPR images of LiNc-BuO:PDMS chip

formulations. Distribution of spins was evaluated using X-band EPR imaging. Samples were imaged under anoxic condition, in a sealed tube. Image intensity correlated directly with the normalized spin density results shown in **(a)**. Images demonstrate high-degree of uniformity in the distribution of LiNc-BuO spins within the PDMS matrix in all four formulations

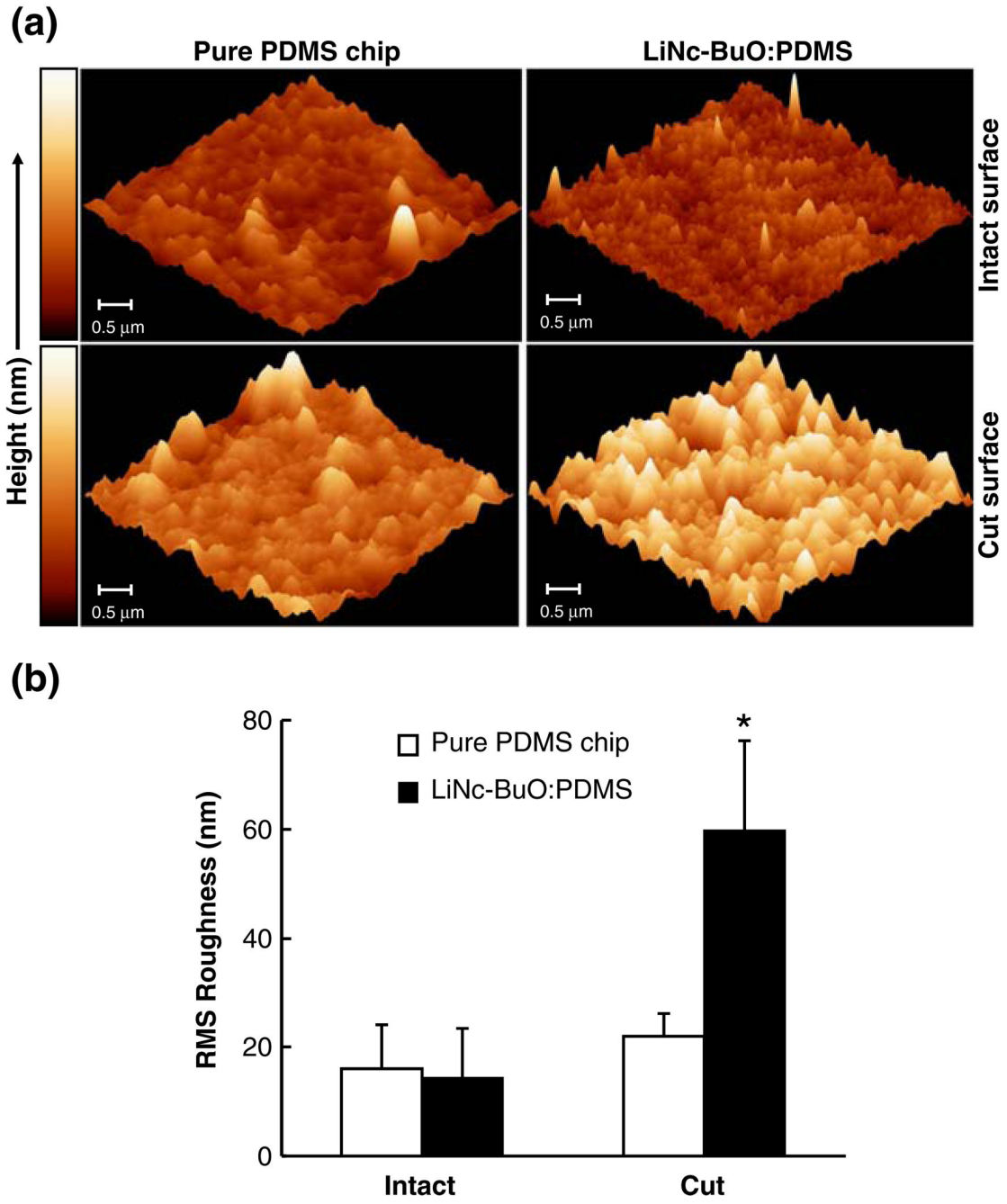

Fig. 3.

Surface evaluation of a LiNc-BuO:PDMS chip using AFM. **(a)** Representative images of the intact (top row) and sectioned (bottom row) surfaces of a pure PDMS chip (no LiNc-BuO crystals, control) and the LiNc-BuO:PDMS chip (40 mg LiNc-BuO in 5.5 g PDMS) are shown. The shade of color in the image represents the height of the surface features (in nm), which is represented by the scale on the left of the image set. The darker color corresponds to valleys, while peaks on the sample surface are represented by the brighter shade of color. The composite image indicates that there was no visually significant difference between the intact surface of the pure PDMS chip and the LiNc-BuO:PDMS chip. However, an increase in color brightness, indicating an increase in surface irregularity, was observed for the cut (sectioned) surface of

the chip, compared to the cut surface of the pure chip. **(b)** Quantification of surface roughness, using the roughness analysis tool in the software, indicated a similar trend as the representative images in Panel (a). Data are represented as mean ± SD (n=6). No significant difference in RMS roughness was observed between the intact surfaces of the pure PDMS chip and the LiNc-BuO: PDMS chip. However, a statistically significant (p<0.05) increase in RMS roughness was observed for the cut surface of the chip, compared to respective control (cut pure PDMS chip). Results, collectively, indicate non-exposure of embedded LiNc-BuO crystals at the intact surface of the LiNc-BuO:PDMS chip

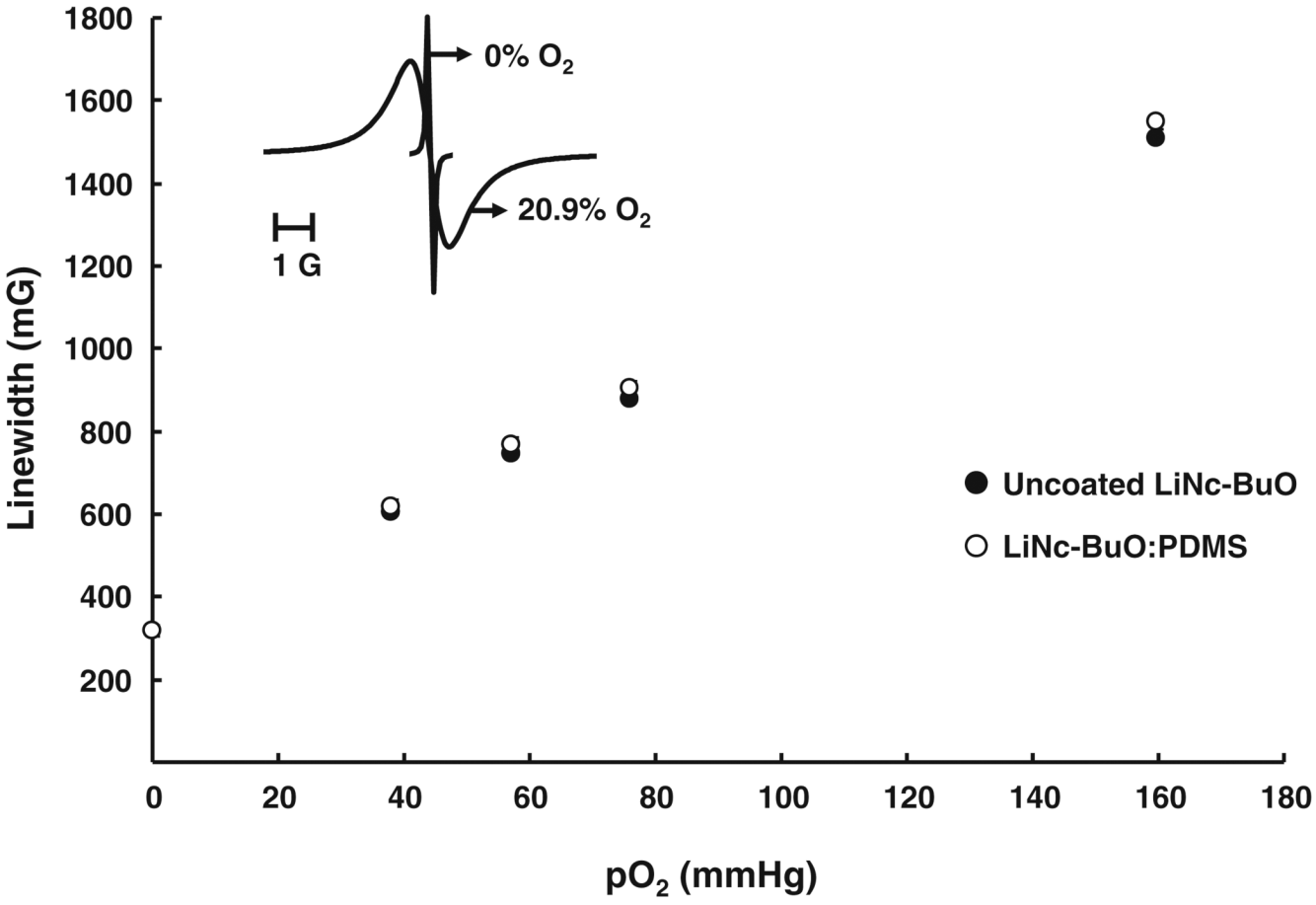

Fig. 4.

Oxygen response of LiNc-BuO:PDMS chip. Oxygen-calibration curves were constructed using peak-to-peak EPR linewidths of uncoated LiNc-BuO (control for comparison) and a LiNc-BuO:PDMS chip (10 mg LiNc-BuO in 5.5 g PDMS) at different partial pressures of oxygen (0–160 mmHg), obtained using X-band EPR spectroscopy. The plot shows a linear relationship between linewidth and pO_2 for both uncoated LiNc-BuO and the chip, which was reversible and reproducible, in each case. This relationship can be represented by the expression: $LW = LW_0 + m * pO_2$, where LW = linewidth (mG), LW_0 = anoxic linewidth (mG, intercept of the curve), m = oxygen sensitivity (mG/mmHg, slope of the curve), and pO_2 = oxygen partial pressure (mmHg). Each data point represents mean ± SD (*n*=3) of linewidth, at that particular pO_2. The oxygen sensitivity of LiNc-BuO: PDMS (7.65±0.07 mG/mmHg) was not significantly different from that of uncoated LiNc-BuO (7.54±0.10 mG/mmHg). Results indicate that the coating procedure did not have an adverse effect on the oxygen-sensing properties of the encapsulated LiNc-BuO. **(Inset)** EPR spectra of LiNc-BuO:PDMS recorded at X-band (9.8 GHz). Spectra obtained under 100% N_2 (0% O_2, anoxic condition) and in the presence of 20.9% O_2 (room air) are shown

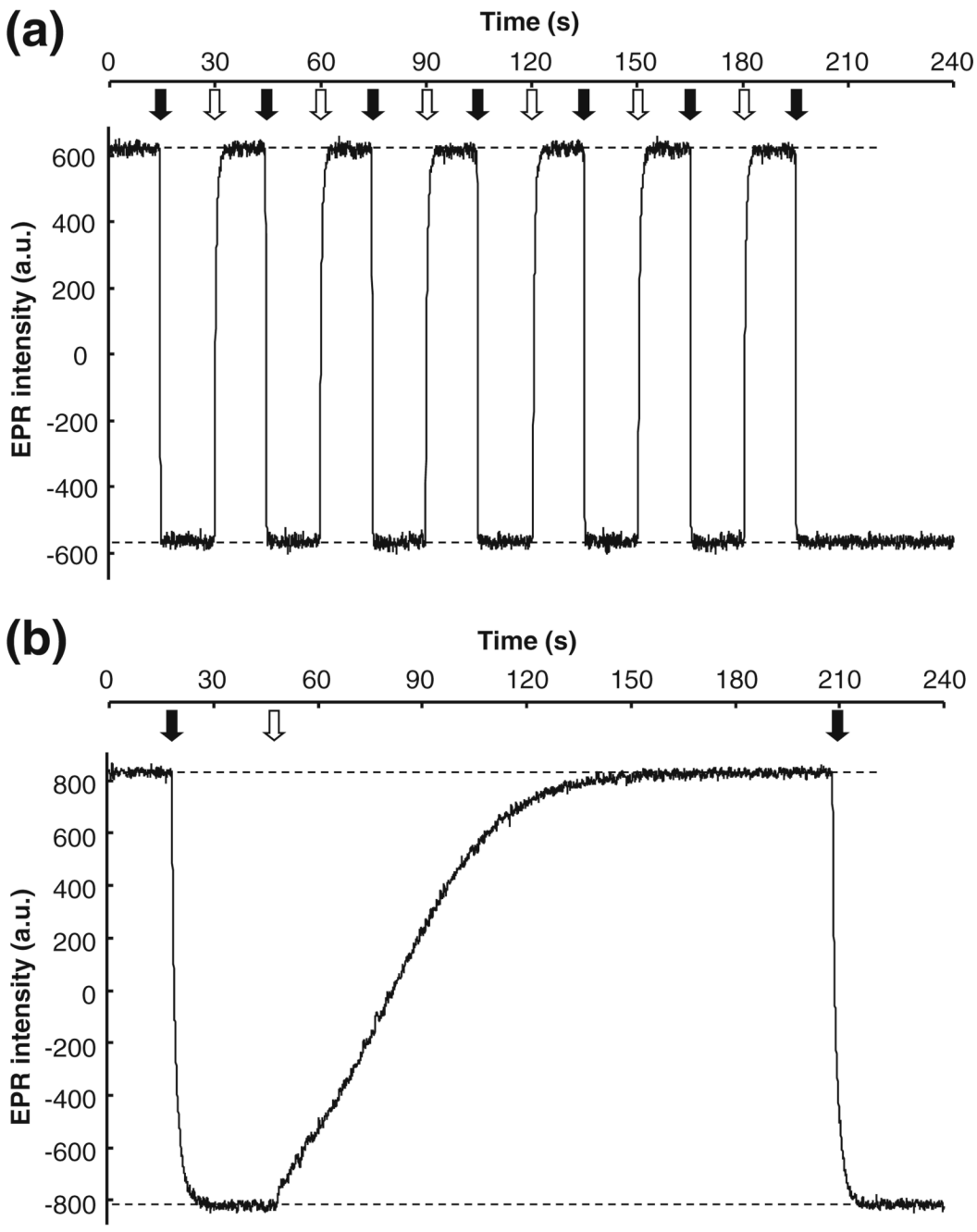

Fig. 5.

Temporal response of LiNc-BuO:PDMS chip to changes in oxygen partial pressure. Effect of oxygenation/deoxygenation on the EPR response of LiNc-BuO:PDMS was measured at X-band (9.8 GHz). Chips made by the encapsulation of 40 mg of LiNc-BuO in 5.5 g of PDMS were used, while uncoated LiNc-BuO was used as a standard for comparison. The samples were equilibrated with nitrogen and the magnetic field was set at the peak of the EPR spectrum under anoxic condition (preset). The response of the EPR signal to rapid switching of the perfusing gas, from nitrogen (0% O_2) to room air (20.9% O_2), was monitored and recorded. The time point when room air is introduced is indicated by the filled arrow, while switching to nitrogen is indicated by the clear arrow. The Y-axis of each panel represents the EPR intensity

(in arbitrary units) at the preset magnetic field (peak of the anoxic EPR spectrum) **(a)** Response of uncoated LiNc-BuO. It can be observed that the unencapsulated probe is characterized by rapid switching times (Pandian et al. 2006); of less than a second when switching from nitrogen to room air and approximately 3 seconds when switching from room air back to nitrogen. **(b)** Response of LiNc-BuO:PDMS chip. The chip response was markedly slower compared to uncoated LiNc-BuO. The switch from nitrogen to room air was relatively fast (~5 s), but the switch from room air to nitrogen took significantly longer (~120 s)